JET-P(95)65

On Ion Temperature Profile Measurements in ITER by means of Neutron Spectroscopy

T Elevant[1], H Brelén, P Linden[2], J Scheffel[1].

JET Joint Undertaking, Abingdon, Oxfordshire, OX14 3EA, UK.
[1] Alfvén Laboratory, Royal Institute of Technology, Stockholm, S-10044, Sweden.
[2] Department of Reactor Physics, Chalmers University of Technology, S-412 96 Göteborg, Sweden, (EURATOM/NFR Fusion Association)

Preprint of a Paper to be submitted for publication in
Fusion Technology

November 1995

ABSTRACT

In the next generation of magnetic fusion experiments, such as ITER, information on ion temperature profiles will be needed for burn optimisation and transport studies. The feasibility of obtaining these profiles for the core plasma (r<0.75a) directly from the width of measured 14-MeV neutron energy spectra is demonstrated for Maxwellian ion distributions. Neutron energy spectra and fluxes are calculated using the Monte-Carlo technique. Reaction kinematics and velocity distribution of the reacting ions are taken into account enabling resulting neutron flux and energy distribution, entering a defined collimator, to be calculated. Energy spectra of neutrons emitted along a line-of-sight are obtained by adding the contributions from a large number of sub-volumes. The associated correction factor (peak temperature/line-of-sight measured temperature) depends on the ion temperature itself and is insensitive to variations in temperature-, density- and magnetic flux profiles. The resulting accuracy in the evaluated ion temperature profiles is expected to be better than ± 10%. However, this can be improved to ± 5% provided the ion density profile shape is known. The relative accuracy is estimated to ± 5%.

Features of several spectrometer candidates are briefly described in relation to ITER conditions and measurement requirements. A Time-of-Flight neutron spectrometer is outlined. Experiments with a test device confirm the calculated energy resolution and separation of neutron from gamma events. The spectrometer is shown to be applicable to ITER under both ohmically heated and ignited conditions. A feed-back system will be used to control the detector count-rate at high neutron flux levels to accommodate the large dynamic neutron flux range from $5 \cdot 10^6$ to $5 \cdot 10^{10}$ n/(cm^{2}s). An array of 5-9 Time-of-Flight spectrometers provides ion temperature profiles satisfying ITER measurement requirements, i.e. $T_i \geq 2.5$ keV, 10% accuracy and spatial and temporal resolutions of 30 cm and 100 ms respectively.

I. INTRODUCTION

In the next generation of magnetically confined fusion grade plasma experiments, such as ITER[1] (International Thermonuclear Experimental Reactor), neutrons will be generated through reactions between deuterium and tritium fuel ions. Plasmas with central ion temperatures ranging from 4 to 50 keV, central fuel ion densities from $0.2 \cdot 10^{20}$ to $2 \cdot 10^{20}$ m^{-3} and with volumes of hundreds of m^3, will generate 10^{17} to $5 \cdot 10^{20}$ neutrons per second. The motions of the reacting ions will give rise to Doppler broadenings and shifts in the neutron energy spectra. A Maxwellian ion distribution generates a Gaussian shaped neutron spectrum with its energy spread directly related to the ion temperature, see Appendix. Evaluation of the width of a spectrum recorded by a neutron spectrometer therefore provides a simple and direct means to derive the ion temperature. The reaction rate depends strongly on the temperature and is also proportional to the square of the fuel density. Thus, information contributing to all factors of the important fusion triple products ($n_f T_i \tau_E$, i.e. fuel density, ion temperature and energy confinement-time) is obtainable through measurements of the energy distribution and emission rate of the neutrons. For a recent review article on neutron diagnostics on contemporary experiments see Ref.[2].

Conventional diagnostics, based on non nuclear techniques, may provide the necessary information on the fusion triple product. However, diagnostics based on neutron measurements will become increasingly important in ITER-like devices for several reasons; Firstly, the width of neutron energy spectra will be a simple and direct measure of the ion temperature for most of the operations. Secondly, the ITER neutron emission rate will exceed that of present tokamaks by orders of magnitude and extraction of information with improved spatial and time resolution from the neutron fluxes and energy spectra will therefore be made possible. Thirdly, the high levels of ionisation radiation will induce noise and damage in other diagnostics.

The feasibility of evaluating ion temperature profiles from analysis of neutron energy spectra is here investigated with respect to measurement requirements and conditions at ITER. To make the extracted information on ion temperature profiles useful, time resolutions significantly shorter than energy confinement times must be obtained. This is in the order of a second in today's experiments, e.g. at JET, and is predicted to become a few seconds in ITER. Ion temperature and density profile data will be used for burn optimisation, particle and energy transport studies. Measured profiles will therefore be compared with results obtained from transport model calculations. The gradients of the temperature and density are of particular importance in this type of analysis. Diagnostic requirements for ITER have been specified and are partially described in Sec. II. The special measurement conditions given for ITER are briefly described in the same section. Neutron fluxes and energy spectra have been calculated by means of the Monte-Carlo technique, which takes into account the kinematics of the

reaction and the velocity distribution of the reacting ions. The calculations and the results, including a small correction factor due to the line-of-sight integrated measurements, are described in Sec. III. It is shown that the accuracy of the derivation of an ion temperature profile improves when neutron flux information is taken into account. Sec. IV provides a summary of the spectrometer requirements in terms of statistics and energy resolution. Capabilities of different spectrometers with respect to energy resolution, efficiencies and count-rates are briefly described. Particular attention is given to anticipated performance with respect to the ITER environment and diagnostic requirements. A purpose designed, partially tested, time-of-flight spectrometer is briefly described in Sec. V. The applicability of an array of 5 such spectrometers is demonstrated for major ITER operating phases in the same section. Thanks to their high degree of flexibility, well-designed spectrometers of this type can provide ion temperature profiles satisfying the ITER diagnostic requirements both under ohmic heating and ignited conditions.

II. ITER DIAGNOSTICS

To make measurements for both control and physics studies of plasmas in ITER, a comprehensive set of diagnostics has to be used[1,3,4]. Some represent upgraded versions of conventional methods and others are based on techniques not yet proven. The conditions under which the diagnostics will operate are particularly difficult due to high levels of electromagnetic and ionising radiation.

II.A. Diagnostic requirements

Burn optimisation and plasma transport studies are the main incentives for ion temperature profile measurements. Requirements for ITER diagnostics for various measurements have been identified[3,4]; in particular, ion temperatures from 0.5 to 50 keV have to be measured. The low temperatures outside r = 0.75a, will be measured by optical methods. Predictions of density and temperature profiles yield $n_e(r)=n_e(0)[1-(r/a)^2]^{0.5}$ and $T_i(r)=T_i(0)[1-(r/a)^2]^{1.0}$, respectively[4]. The requirements on T_i measurements by means of neutron spectroscopy can be summarised:

T_i ranging from:	2.5 to 50 keV,	accuracy :	$dT_i/T_i < 10\%$,
temporal resolution:	Δt = 100 ms,	spatial coverage :	$r \leq 0.75a$,
spatial resolution:	Δr = 30 cm.		

To get a complete picture of the ion temperature profile some overlap of the regions for nuclear and non-nuclear methods is foreseen.

Transport models are generally very sensitive to relative values in temperatures and densities. For accurate comparisons between calculations and measurements, a relative accuracy of 3%, time resolution of 50-100 ms and one radial point measurement every 15 cm must be obtained for the ion temperature profile measurements[5,6].

II.B. Measurement conditions

The measurement conditions will be particularly difficult at ITER due to high levels of ionising and electromagnetic radiation. Furthermore, severe constraints are applied to the first wall and the blanket by the cooling system. Therefore, the sizes of penetrations are restricted to small cross-section areas. The space just outside the torus ports will be occupied by equipment that must be close to the torus such as cooling tubes, heating equipment and lines-of-sight tubes for various diagnostics. The ports will also be used for access for exchange of blanket modules and for inspections. The access near the ports for diagnostics is therefore limited. The torus will be surrounded by a main shielding placed at a distance of approximately 20 m from the centre of the torus, i.e. 10-12 m from plasma centre. Due to induced radiation inside the shielding, remote handling has to be employed for maintenance and restoration of equipment. Therefore, instruments that can operate adequately at large distances, such as most of the neutron diagnostics, will preferably be located outside the main shielding.

III. CALCULATIONS OF NEUTRON ENERGY SPECTRA AND FLUXES

Neutron energy spectra generated under different heating conditions have been calculated by means of a Monte-Carlo technique using the NSPEC code[7]. The code takes the reaction kinematics and the velocity distributions of the reacting ions into account and calculates the resulting energy distribution and fluxes, Φ_n, of neutrons defined by a collimator. Energy spectra of neutrons emitted along a line-of-sight are obtained by adding the contributions from a large number of sub-volumes. The fusion cross-sections given in Ref.[8] are used.

The width of neutron energy spectra, originating from fusion reactions between Maxwellian distributed ions, is a direct measure of the ion temperature[9]. However, profile shapes influence energy spectra when neutrons emitted along a line-of-sight in a thermonuclear plasma are observed. To estimate the value of the associated correction factor, a number of simulations using different ion temperature and density profiles have been carried out for ohmically heated and ignited D(50%)-T(50%) plasmas in ITER geometry.

III.A. Determination of ion temperature profiles

Calculated correction factors for evaluation of ion temperatures are shown in fig.1. They yield the maximum ion temperature along a line-of-sight T_i^{max}, when multiplied with the observed

ion temperature T_i^{obs}. If the magnetic equilibrium $\psi(r,z)$ is known, $T_i(\psi)$ can be obtained taking the line-of-sight geometry into account. Consequently, the coefficient β in an assumed median plane profile of the form $T_i(r) = T_i(0)[1 - (r/a)^2]^\beta$ can be derived. Similarly we employ density profiles of the form $n(r) = n(0)[1 - (r/a)^2]^\alpha$. It is obvious from fig. 1 that the correction factor is profile dependent. The top full line, with $(\alpha,\beta)=(0.05,2.0)$, represents an extreme case where the density profile is nearly flat, giving large neutron contributions from regions outside the temperature maximum. The lower full line shows an other extreme where $(\alpha,\beta)=(1.0,0.5)$, i.e. the density is peaked and the temperature profile is fairly flat. The central curve represents standard ITER parameters[4]: $(\alpha,\beta)=(0.5,1.0)$. One encouraging fact is illustrated in fig. 1: even if the density and temperature profiles are completely unknown, the maximum temperature along each line-of-sight can be derived from the measured T_i with an accuracy better than 10%.

For temperatures given in keV, the correction factor can be given the following analytical form when fitted to code data:

$$C(T_i^{obs}) = 1.06 + (0.003 \pm 0.003)T_i^{obs} \qquad (1)$$

The results clustered along each line in fig. 1 correspond to data from four different lines-of-sight that all pass through a pivot point in the median plane at R=12 m. The lines-of-sight intersect a vertical line passing through the magnetic axis at 0, 1, 2 and 3 m above the geometric centre axis respectively. Hence, the results are independent of the particular line-of-sight chosen. For evaluations of ion temperature gradients, errors in the line integral corrections are therefore cancelled and the relative accuracy is estimated to $\pm$ 5%.

In order to estimate the sensitivity of the correction factor on deviations from the true $\psi(r,z)$, we have computed $C(T_i^{obs})$ for the ITER standard equilibrium, i.e. R_{min}=5.0 m, R_0=8.0 m, R_{max}=11.0 m, Δ_{Shaf}=0.5 m, κ=1.6 and z_{axis} (height above magnetic axis)=4.8 m, as indicated by the full lines in fig. 1. The dashed lines represent an inverse-D shaped ITER equilibrium with Δ_{Shaf}=0.3 m, κ=1.6 and z_{axis}=4.3 m. The reasons for the small differences in $C(T_i^{obs})$ are that only lines-of-sight within r=0.75a are considered here, making flux shape effects small, and that contributions to the neutron flux are small near the periphery. An important consequence for ITER is that the complicated flux geometry near the divertor x-points does not require advanced modelling for estimates of neutron emissions.

III.B. Temperature corrections using flux measurements

The accuracy needed for transport studies, see Sec.II.A, justifies efforts to determine ion temperature profiles with high accuracy. This can be achieved by including information on neutron fluxes, e.g. by using a neutron flux detector at the collimator end. Given the ion temperature profile shape β, measurement of flux ratios for different lines-of-sight

$R_{\Phi_n} = \Phi_n(z=0)/\Phi_n(z=3)$, see fig. 2, provides information on plasma density shape, i.e. α, as illustrated in fig. 3. Here $\Phi_n(z)$ denotes the neutron flux into a collimator with a line-of-sight intersecting a vertical line through the magnetic axis at a distance z above the horizontal mid-plane. The curves correspond to specific on-axis ion temperatures as indicated and are based on the same profiles as in fig. 1. The weak variation in flux ratio for the cases $(\alpha,\beta)=(1.0,0.5)$ and $(\alpha,\beta)=(0.5,1.0)$ is confirmed. Obviously, the flux ratio R_{Φ_n} can provide estimates of α for low ion temperatures. At very high temperatures $\alpha+\beta$ becomes a sensitive function of R_{Φ_n}, and the estimates become more sensitive to inaccuracies.

Supposing α could be obtained from R_{Φ_n} measurements (preceded by measurements of ion temperature profile), results shown in fig. 1 may be used to qualify the estimate of β first made. As an example, assume $\alpha+\beta = 1.5$ is obtained from fig. 3. Using the results shown in fig. 1, the uncertainty in the ion temperature evaluation is brought down to ±5%.

The above discussion serves to clarify the principal method for determining the ion temperature profile with high accuracy using neutron diagnostics. For real measurements a numerical algorithm for determination of profile parameters by fitting experimental temperature and density data to precalculated results will be used.

IV. MEASUREMENTS OF NEUTRON ENERGY SPECTRA

For measurements of neutron energy spectra given in Sec. III. and the consequent evaluation of the ion temperature profiles, several spectrometer candidates have been suggested. These are here briefly described with respect to; required statistics, neutron fluxes available, inherent efficiency and energy resolution. ITER measurement requirements and detector radiation damage are also considered.

IV.A. Statistics and resolution for T_i measurements

Energy resolution requirements depend on the width and shape of the neutron energy spectrum to be measured. In cases when the reaction contribution from the Maxwellian ion distribution is dominant, the neutron energy spectrum is Gaussian shaped. Provided the response function of the instrument also is Gaussian, the accuracy in ion temperature measurements is given by [10]:

$$dT_i/T_i = \{ 2/N_S[(R/W)^2+1]^2 + 4(R/W)^4 (dR/R)^2 \}^{1/2} \qquad (2)$$

where N_S is the number of observations, W the actual width of the neutron spectrum, R the instrumental resolution and dR its accuracy, see also Appendix. Using a calibration neutron generator with a Gaussian energy distribution and an energy width equal to 50 keV [FWHM] known to 1% accuracy, dR/R can be determined with 1% accuracy provided the spectrum

contains $6\,10^4$ events, see Appendix. For a well-calibrated spectrometer, eq. (2) gives the minimum required number of observations as a function of ion temperature for energy resolutions of 1.5%, 2.5% and 3.5% (FWHM) and for $dT_i/T_i = 10\%$ as shown[11] in fig. 4. Approximately 600 spectrum events are needed for an instrument with a 1.5% energy resolution when resolving an ion temperature of 2.5 keV.

IV.B. Spectrometers considered

The types of spectrometer considered for the ion temperature profile measurements include simple n-p scattering arrangements using single polyethylene foils, variants of Time-of-Flight (ToF) spectrometers, Magnetic Proton Recoil (MPR), detectors based on silicon- and diamond diodes and scintillating fibres. Table 1 shows the characteristics of spectrometers considered.

Table 1. Operating ranges for spectrometers located outside the ITER main shield.

Spectrometer type	Efficiency (cm^2)	Energy resolution (%, FWHM)	Oper. range T_i (keV)	Oper. range $\phi_{n,max}/\phi_{n,min}$	Radiation damage, at G_{max} (n/cm^2) [3]	Dimensions W H L (m^3)
Large spectrometers						
Proton recoil [12]	10^{-4}	2.2	≥5	$5\cdot10^9/5\cdot10^7$	10^{15} [3a]	0.4,0.4,2
Time-of-Flight [13]	10^{-3}	1.6	≥2.5	$5\cdot10^{10}/5\cdot10^6$	10^{16} [3b]	1,1,4
Associated particle, Time-of-Flight [14,15,16]	10^{-5}	1.5	≥7	$5\cdot10^{10}/5\cdot10^8$	10^{15} [3a]	2,2,1
Magnetic proton recoil [17]	$5\cdot10^{-5}$	2.5	≥7	$5\cdot10^{10}/10^8$	10^{16} [3b]	1,2.5,1
Proton recoil with micro channel [18]	10^{-5}	2	≥7	$5\cdot10^{10}/10^8$	$5\cdot10^{15}$ [3a]	0.2,0.2, 0.4
Compact spectrometers						
Silicon diode [19]	10^{-3}	0.8	2-20	— [2]	10^{12} [3c]	Small
Diamond diode [20]	10^{-5}	2.0	≥5	$2\cdot10^9/5\cdot10^8$	$1\text{-}5\cdot10^{14}$ [3c]	Small
Scintillating Fibre detector [21]	$3\cdot10^{-3}$	3.3	≥7	$10^8/10^6$	$7\cdot10^{15}$ [22, 3d]	Small

[1] Fulfilling $\Delta t \leq 100$ ms. [2] Due to intrinsic spurious reactions the best obtainable time resolutions is 250 ms. [3] Numbers refer to fluence in neutron beam and are given by damage in [23]: [3a] silicon diode outside neutron beam, [3b] polyethylene foil in neutron beam, [3c] diodes in neutron beam, [3d] scintillating fibres in beam.

Operating ranges are given for which the ITER diagnostic requirements are fulfilled for spectrometers located outside the main shielding and with fluxes and efficiencies taken into account. Temperature and density profiles are as given in Sec. II. Estimates of fluences causing radiation damages are based on a ratio equal to 10^3 for flux in the neutron beam over flux at a position 2-5 cm outside the neutron beam. At a distance of 15 cm this ratio is equal to 10^4, see Sec.V.B.

A brief description is here given for each of the techniques which all measure energy distributions of collimated neutrons;

Proton recoil: The technique utilises (n,p) elastic scattering in a thin annular polyethylene foil. Recoil proton energies are measured in a silicon diode located a few cm outside and at an angle of $\pi/18$ relative to the neutron beam. Geometric restrictions enable the energies of the original neutrons to be determined[12]. A tandem configuration is used, providing a simple and cost-effective spectrometer. The energy resolution can be improved only with reduced efficiency. For an energy resolution of 2.2% the operating range is restricted to $T_i > 5$ keV due to the product of neutron flux and detection efficiency, see section IV.A.

Time-of-flight: Neutrons undergo elastic scattering in a thin polyethylene foil. Neutrons scattered through an angle $\pi/4$ are detected in a thick fibre scintillator detector placed a few meters from the neutron beam. The recoil protons are detected in a thin scintillator fibre detector located at a few cm from the neutron beam. Elapsed time durations between correlated events are recorded and the energies of the original neutrons are evaluated[11,13]. By increasing the detector area the energy resolution can be improved with maintained efficiency. For an energy resolution of 1.6%, operating range is allow for measurements of $T_i > 2.5$ keV due to the product of neutron flux and detection efficiency.

Associated particle time-of-flight: Neutrons undergo elastic (n,p) scattering in a polyethylene foil aligned with an almost parallel neutron beam. The recoil protons are detected in silicon diodes placed 5 cm from the foil at an angle of $\pi/9$ radians. The neutrons are detected in a set of scintillators located approximately one m from the neutron beam. Time durations elapsed between correlated detected neutron and proton events are recorded together with the energies of the recoil protons. The energies of the original neutrons are thereafter determined[14,15,16]. The energy resolution can be improved only with reduced efficiency as a consequence. For given energy resolution, operating range is restricted to $T_i > 6$ keV due to the product of neutron flux and detection efficiency.

Magnetic proton recoil: Neutrons undergo (n,p) elastic scattering in a thin polyethylene foil. Forward directed recoil protons are deviated by a magnetic field and detected dispersively in a set of scintillators located a few m from the neutron beam. The energies of the original neu-

trons are determined from the position of detection[17]. The energy resolution can be improved only with reduced efficiency. For given energy resolution, operating range is restricted to $T_i >$ 7 keV due to the product of neutron flux and detection efficiency.

Proton recoil with micro-channels: The technique utilises (n,p) scattering in a thin annular polyethylene foil[18]. Recoil proton energies are measured in silicon diodes located 15 cm outside and at an angle of $\pi/6$ radians relative to the neutron beam. A micro-collimator plate is used to define the solid angle of recoil protons. The energy resolution can be improved only with reduced efficiency. For given energy resolution, operating range is restricted to $T_i > 7$ keV.

Silicon diode: Neutrons undergo intrinsic $^{28}Si(n,\alpha)^{25}Mg$ and $^{28}Si(n,p)^{28}Al$ reactions in a silicon diode placed in the neutron beam. Released energies are deposited in the diode and the energies of the impinging neutrons are determined[19]. Due to saturation caused by intrinsic background events this detector provides in practice a time resolution of approximately 200 ms.

Diamond diode: The technique utilises intrinsic $^{12}C(n,\alpha_0)^{9}Be$ reactions in a diamond diode placed in the neutron beam. Released energies are deposited in the diode and the energies of the impinging neutrons are determined[20]. Due to saturation caused by intrinsic background events this detector provides a time resolution of approximately 25ms.

Scintillating fibre detector: Alternate orthogonal planes of thin square scintillating fibres form a compact detector. The fibre axes are oriented perpendicular to the incident collimated neutron beam direction. Neutrons undergo elastic (n,p) scattering, and the pattern of fibres fired provides a measure of the proton range and recoil angle of the proton and therefore of the energy of the incident neutron. Different specific light output from protons and electrons enables neutron and gamma events to be separated by means of pulse amplitude discrimination. The fast response of the scintillating fibres enables maximum useful count-rates of 500 kHz to be obtained. Results from neutron and gamma transport calculations for a similar neutron detector are given in ref. [24].

V. RADIAL ARRAY OF TIME-OF-FLIGHT SPECTROMETERS

The time-of-flight technique combines a large operating range with high resistance against radiation damages, and high degree of flexibility[11,13]. A version suitable for 2.45 MeV neutrons has provided information on high energetic ions and ion temperatures in the JET tokamak[25,26,27]. Together with the moderate weight (~ 400 kg) this makes the time-of-flight spectrometer a suitable instrument fulfilling all ITER plasma measurement requirements. A brief description of the instrument is here followed by a discussion on the applicability of a

radial array of spectrometers purposely designed for measurements of ion temperature profiles. For maximum count-rates and background considerations, see Appendix.

V.A. Time-of-flight neutron spectrometer

The time-of-flight spectrometer proposed for measurements of well-collimated neutrons is described in Ref.[13]. It is based on (n,p) elastic scattering in a polyethylene foil. The recoiled proton is detected in a detector D_0, that is located at a distance of 3-4 cm outside the neutron beam. The scattered neutron is detected in another detector D_1, located at a distance of 4.5 m from the foil and 3 m from the neutron beam, see fig. 5. The elapsed time between the two detection events is recorded and used in the neutron energy evaluation. Scintillating fibres and photo-multiplier tubes are utilised in the two detectors. The D_0 detector has two signal channels and the D_1 has eight channels. The foil is oriented along the neutron beam and the average neutron scattering angle is chosen to $\pi/4$. A combination of narrow neutron collimator (i.e. 0.5•10 cm^2) and large foil volume (i.e. 10•24•0.03 cm^3) is used. An array of apertures, placed between the foil and the D_0 detector, selects protons with the recoil angle around $\pi/4$ and thereby prevents the detector being encumbered with non-relevant proton events.

Calculations of the neutron transport in the spectrometer have been made by means of Monte-Carlo simulations[13], and the results are provided in table 2 and 3.

Table 2. Neutron transport calculations for a ToF-spectrometer

Energy resolution	1.6	[%,FWHM/E_n]
Neutron energy range	11-18	[MeV]
Efficiency	10^{-3}	[cm^2]

Table 3. Performance for a ToF-spectrometer located outside the main shielding.

Spectrometer count-rate	at $\Phi_n = 5\cdot10^6$ [1]	n/(cm^2 s)	$5\cdot10^3$	[c/s]
	at $\Phi_n = 5\cdot10^{10}$ [2]	n/(cm^2 s)	$1\cdot10^6$ [3]	[c/s]
Time resolution for evaluation of $T_i > 2.5$ keV	at $\Phi_n = 5\cdot10^6$	n/(cm^2 s)	100	[ms]
	at $\Phi_n = 5\cdot10^{10}$	n/(cm^2 s)	5	[ms]
D_0 count-rate	at $\Phi_n = 5\cdot10^6$	n/(cm^2 s)	$2\cdot10^4$	[c/s]
	at $\Phi_n = 5\cdot10^{10}$	n/(cm^2 s)	$4\cdot10^6$	[c/s]
D_1 count-rate	at $\Phi_n = 5\cdot10^6$	n/(cm^2 s)	$1\cdot10^4$	[c/s]
	at $\Phi_n = 5\cdot10^{10}$	n/(cm^2 s)	$3\cdot10^6$	[c/s]
Maximum acceptable background flux at D_1	E_n in MeV range		$1\cdot10^4$	[n/(cm^2 s)]
	E_γ in MeV range		$1\cdot10^4$	[γ/(cm^2 s)]

Correspond to flux levels of: [1] ohmically heated plasmas, and [2] ignited plasmas. [3]An automatic control scheme for reduction of scatter foil volume will be used at high fluxes, see Sec. V.D.

The high efficiency enables operation at large distances from the plasma, i.e. outside the main radiation shielding.

V.B. Neutron transport in a purpose designed collimator

Extensive neutron transport calculations have been carried out for a collimator designed for a similar 14-MeV spectrometer to be used at JET[28]. Same collimator geometry will be used for the ITER-ToF spectrometer. A three dimensional Monte-Carlo code[28] has been written for calculations of neutron transport studies in long collimators. The geometry is described correctly while approximate values of the cross-sections and scattering functions have been used. The main contribution to the scattered flux in straight collimators is caused by scattering in the collimator surface[29]. A dual tapered collimator, shown in fig. 5, will therefore be used. Two principles are governing the design; Firstly, the end nearest to the neutron source is tapered with an angle such that there is no direct line-of-sight from that part of the collimator surface to the scatter foil or detectors. Secondly, the end nearest to the detector is tapered with an angle such that there is no direct line-of-sight from the neutron source to the surface of that part of the collimator.

Results from flux calculations are shown in figs. 6a) and b) where the fluxes are normalised to 10^9 n/(cm^{2}s) at the centre of the scatter foil. The flux distributions across and along the slit (with waist dimensions 10 ·0.5 cm^2) are shown in fig. 6a and fig. 6b respectively. The total neutron flux has a well-defined step of three decades at the beam edge that shows that the foil is evenly irradiated and efficiently used. The ratio of scattered flux over total flux at the foil position is less than 0.5%.

V.C. Tests of detectors

Experiments with a simple test device consisting of one scintillator (1•1•2.5 cm^3) and one fibre detector with 20 fibres (0.2•0.2•70 cm^3) have been performed. System timing resolution of 0.9 ns has been measured by means of a ^{60}Co gamma source, see fig. 7. Timing resolution contributes by 75% to the over-all energy resolution, and the result is consistent with an energy resolution of 1.6%(FWHM). Furthermore, pulse amplitudes from neutrons with energies up to 10 MeV and gamma rays with energies from 0.5 to 1 MeV have been recorded. Pulse height ratios of 20/6/1 for (neutron-signal) / (gamma-signal) / (noise) events, have been measured. The result demonstrates the feasibility of a simple pulse amplitude discrimination for separation of neutron and gamma signals, which is of particular importance for reducing the random background. Similar results have been obtained by Ref.[24]. Energy spectra of 14-MeV neutrons have also been measured which demonstrates the feasibility to use the spectrometer for measurements of neutrons from deuterium-tritium plasmas.

V.D. Automatic control scheme for adjustment of spectrometer count-rates

The wide range in expected neutron flux, as shown in table 3, will present a problem with unseparable coincidences at the higher end and too low statistics at the lower end. To overcome these difficulties it is proposed that the volume of the scatter foil exposed to the incoming neutron flux is varied actively so that the flux of recoil protons in the D_0 detector is kept at a constant level. The variation in volume will be achieved by means of angular or translational movements. The details of the mechanism for these movements will be designed at a later stage. Whichever principle is chosen the movements required for keeping the recoil proton flux constant are produced by an automatic control system as shown in fig. 8. The output signal, i.e. the flux of recoil protons detected by the D_0 detector, is fed back and compared with the constant reference value representing the required count-rate in the same detector. The difference between these two signals is then used in the controller to generate the actuation of the movements in the attempt of keeping this difference to a minimum. If the device moving the scatter foil is driven by a servo motor or contains some other integrating element, the controller is suggested to be of proportional derivative (PD) type. Otherwise an integration should be included in the controller function for accuracy reasons.

The scatterer acts as a multiplier making the gain in the control loop depend on the incoming neutron flux. A controller designed for the highest specified flux, i.e. highest loop gain, will show low performance at low neutron flux. Vice versa, a case designed to give acceptable performance at low neutron flux will most likely develop an instability at higher neutron flux. A simulation was carried out to illustrate the previous case with a conservatively designed controller. For the purpose of this simulation the total neutron flux is set to vary as a triangular wave with a maximum slope of $5 \cdot 10^8$ n/(cm^{2}s^2). The maximum and minimum flux levels, given in table 3, are shown in Figs.9 and 10 respectively. These figures also show how the count-rate in the proton detector is controlled at the requested value. The transient at the lower turning point at low neutron flux has, as expected, far more impact on the controlled flux than that at the upper turning point.

In order to improve the control performance at the lower neutron flux without deteriorating the performance at the higher, a gain schedule based on the neutron flux is introduced as indicated with dotted lines in fig. 8. The neutron flux is assumed to be measured by means of a flux detector located in the collimator, see Sec. III. The gain scheduler controls a factor in the control loop inversely proportional to the total neutron flux, i.e. an elimination of the multiplicative effect from the scatter foil. The control loop is not sensitive to moderate parameter variations and therefore the inversion does not have to be exact. The suppression of this and other parameter variations as well as general disturbances necessitates the introduction of the control system. The inversion function should in any case be kept at a constant value for neutron fluxes below a certain low value.

A repeat of the simulation at low neutron flux with the gain schedule included gives the result shown in fig. 11. Again, the D_O count-rate is kept at requested level. In addition the transients generated by the turning in the neutron flux levels now affects the proton flow to an acceptable degree. The gain scheduled controller produces the same result as obtained at the high neutron flux as shown in fig. 9.

V.E. Array of Time-of-Flight spectrometers

To meet the ITER requirements on ion temperature profile measurements, several lines-of-sight must be utilised. For illustrative purposes, an array consisting of five spectrometers is outlined in fig. 2. This arrangement provides ion temperature measurements for ohmic as well as ignited conditions out to a minor radius of 0.75a, down to ion temperatures of 2.5 keV and with a temporal resolution of 100 ms. Assuming constant ion temperatures on each magnetic flux surface, radial resolution better than 30 cm with 80 cm spacing is provided. To collect the necessary number of counts (i.e. 500) in one spectrum per 100 ms, a minimum flux of $5 \cdot 10^6$ n/(cm^{2}s) is needed, see Sec. IV.A. The otherwise high fluxes in the central lines-of-sight, will be compensated by use of narrow collimators. This will reduce the fluxes by a factor of 8-10 and provide a radial resolution of a few cm for $r < 0.60a$. As shown in the Appendix, the spectrometer maximum count-rate is approximately equal to 10^6 c/s, and the intrinsic neutron flux range is a factor of 200. The maximum fluxes in central collimators will be $5 \cdot 10^9$ to 10^{10} n/(cm^{2}s) which requires a reduction of the scatter foil by a factor 5-10. This implies moving a few grams of foil material a few cm within the time period of 100 ms and will be achieved by means of the automatic scheme described in Sec. V.D.

The number of spectrometers chosen is determined by the desire to have accurate information on the ion temperature profile on one hand and practical considerations such as neutron flux cross-talk between the collimated lines-of-sight and detector space requirements on the other. To allow for a large variety of temperature profiles, we assume that a description of the form $T_i(r) = T_i(0)\,[1-(r/a)^\gamma]^\beta$ is sufficient. However, due to the single-null divertor, up-down symmetry cannot *apriori* be assumed. Thus, the five degrees of freedom must correspond to at least five independent spectrometers.

Utilising the direct procedure for evaluation of ion temperature profiles, described in Sec. III, an array of five time-of-flight spectrometers provides ion temperature profiles with an accuracy of $\pm 10\%$ under both ohmically heated and ignited conditions. Furthermore, by combining measurement of neutron spectra and fluxes and using the iterative procedure described in Sec. III, ion temperature profiles can be determined with an accuracy of $\pm 5\%$. All these measurements fulfil the ITER measurement requirements as described in Sec. II.

VI. CONCLUSIONS

Calculations show the feasibility to derive ion temperature profiles up to r = 0.75a directly from the width of multiple line-of-sight-integrated neutron energy spectra in a fusion experimental reactor like ITER. A correction factor which value is a function of the observed ion temperature T_i^{obs}, must be applied. It can be given an analytical form when fitted to code data. Broad variations in density-, temperature- and magnetic flux surface profile shapes have negligible effects in comparison with the required accuracy in ion temperature measurements.

An array of 5-9 time-of-flight spectrometers, with energy resolution of 1.6%, efficiency of 10^{-3} cm^2 and maximum count-rate of 1 MHz, is outlined. It provides ion temperature profile data also at low temperatures in accordance with the ITER diagnostic requirements; ion temperature range $T_i \geq 2.5$ keV, accuracy 10%, spatial resolution ≤ 30 cm and temporal resolution $\leq$100 ms. With use of information on fuel ion profiles (e.g. through measurements of neutron fluxes), the accuracy in T_i evaluation can be improved to $\pm$ 5%.

VI. ACKNOWLEDGEMENTS

The authors gratefully acknowledge the European working group on ITER neutron diagnostics and in particular Dr. O.N. Jarvis for stimulating discussions. This work has been supported by the European Communities under an association contract between EURATOM and the Swedish Natural Science Research Council.

APPENDIX

A. ANALYSIS OF ERROR IN ION TEMPERATURE EVALUATION

The time-of-flight spectrometer is a coincidence instrument and will therefore generate random background events, which scales as the product of the count-rate in the detectors. Count-rate limitations are investigated particularly with respect to ITER requirements on ion temperature measurements and estimated radiation background.

A.I. General signal- and background considerations

Reacting plasma ions, with a Maxwellian velocity distribution function, will generate an approximately Gaussian shaped neutron spectrum with the ion temperature directly related to the width W, of the neutron distribution[9]. Effects from different contributions to the error in the derived ion temperature T_i, are here quantified. In the following, R denotes the width of the spectrometer response function and M the width of the measured spectrum. From Ref. [9]:

$$W=k_1\ T_i^{1/2} \tag{A1}$$

With W expressed in standard deviations, σ, T_i in keV and applied to deuterium-tritium plasmas, k_1 is equal to 75.3.

An error dW in W propagates into a fractional error in the evaluated T_i:

$$dT_i/(2\ T_i) = dW/W \tag{A2}$$

Provided the spectrometer has a Gaussian response function, which is uncorrelated with the neutron spectrum, T_i is easily derived from eq.(A1) and M after reduction of the intrinsic width R:

$$T_i\ k_1^2 = W^2 = (M^2 - R^2) \tag{A3}$$

Differentiation and squaring of (A3), assuming independent contributions, lead to:

$$(dW/W)^2=[(M^2/W^2)dM/M]^2+(R\ dR/W^2)^2=(1+R^2/W^2)^2(dM/M)^2+(R\ dR/W^2)^2 \tag{A4}$$

where dR is the accuracy of the energy resolution R, derived from a calibration measurement. The error dM in M has two contributions for a Gaussian spectrum with N_S number of events. The first contribution[10] relates to the fractional standard error of the standard deviation of a distribution with finite statistics. This is equal to[30]:

$$dM_S/M = 1/(2\ N_S)^{0.5} \qquad (A5)$$

The second contribution originates from the background counts N_B that causes an uncertainty dN_S, in the number of events to be accounted for in the Gaussian distribution, N_S. For a Maxwellian plasma the spectrum consists only of the Gaussian distribution and a background, and the error $|dN_S|$ is therefore equal to the error $|dN_B|$. For a Gaussian distribution, the number of events is given by[30]:

$$N_S = (2\pi)^{0.5}\ M\ Y_0 \qquad (A6)$$

where Y_0 is the maximum value of the distribution. Differentiation of eq.(A6) therefore gives the fractional error in M due to background counts equal to:

$$|dM_B|/M = |dN_S|\ /N_S = \ |dN_B|\ /N_S \qquad (A7)$$

From eq.s(A5) and (A7) the total fractional error in M becomes:

$$(dM/M)^2 = [1/(2\ N_S)^{0.5} + |dN_B|/N_S]^2 \qquad (A8)$$

Using eq.s (A2), (A4) and (A8), the fractional error in W becomes:

$$(dT_i/(2\ T_i))^2=(dW/W)^2=[1+R^2/W^2]^2\ [1/(2\ N_S)^{0.5}+|dN_B|/N_S]^2+(R^2/W^2)^2\ (dR/R)^2 \qquad (A9)$$

For calibration purposes, the fractional error dR/R can be derived using the same analysis technique as described above. A calibration measurement by means of a neutron beam with a narrow energy width (i.e. $\sigma_n \approx 20$ keV) and $N_C = 6\ 10^4$ counts in the peak, gives dR/R < 1%. For $T_i > 2.5$ keV the last term in eq.(A9) can therefore be neglected and the fractional error in W becomes:

$$(dT_i/(2\ T_i))^2 = (dW/W)^2\ = [1+R^2/W^2]^2\ [1/(2\ N_S)^{0.5}+|dN_B|/N_S]^2 \qquad (A10)$$

A.II. Application to the Time-of-Flight spectrometer

For the special case of a double scattering time-of-flight spectrometer, the random background counts N_B is determined from the number of counts N_0 and N_1 in the two detectors D_0 and D_1 respectively[13]. For a timing window $\Delta\tau$ and a spectrum collection time ΔT, N_B is equal to:

$$N_B = R_B\ \Delta T = R_0\ R_1\ \Delta\tau\ \Delta T = N_0\ N_1\ \Delta\tau/\Delta T \qquad (A11)$$

where R_0 and R_1 are the count-rates in the two detectors. Differentiation of eq.(A11) and assuming uncorrelated error contributions yields the total fractional error in N_B equal to:

$$(dN_B/N_B)^2 = (dN_0/N_0)^2 + (dN_1/N_1)^2 + (d\Delta\tau/\Delta\tau)^2 + (d\Delta T/\Delta T)^2 \qquad (A12)$$

The spectrometer geometry and detector arrangements give $N_0 \approx N_1 \approx \eta\ N_S$. Elastic and inelastic scattering on hydrogen and carbon in the foil cause intrinsic background in the two detectors and yield $\eta \approx 4$. This gives the minimum values of the first two terms in eq. (A12). The last two terms in (A12) are small for $\Delta\tau$ = 30 ns, $d\Delta\tau \leq 0.25$ ns, $\Delta T > 5$ ms, $d\Delta T = 1$ μs and $500 < N_S < 5000$ counts. Thus, from the fractional error in N_0 and N_1, eq.(A12) yields:

$$|dN_B|/ N_B \cong [2/(\eta\ N_S)]^{0.5} \qquad (A13)$$

and therefore

$$|dN_B|/N_S \cong (N_B /N_S^{1.5}) (2/\eta)^{0.5} \qquad (A14)$$

Using eq.s(A10) and (A14) and solving for N_B, the maximum tolerable background becomes:

$$N_B = (N_S/2) (\eta)^{0.5} \{ [dT_i/(2\ T_i)] [W^2/(W^2+R^2)] [2\ N_S]^{0.5}-1 \} \qquad (A15)$$

For dT_i/T_i = 10%, R= 98 keV (σ_R), $\Delta\tau$= 30 ns (corresponding to neutron energies from 11 to 18 MeV) and $\eta \approx 4$, eq.(A15) gives values of N_B presented in the table. Values for three cases of neutron fluxes representing power levels of ohmically- and auxiliary heated and ignited plasmas respectively, are shown in the table.

Φ_n **(n/(cm²s))**	Spectrometer count-rate (c/s)	ΔT (ms)	Spectr. counts N_S (cts.)	T_i (keV)	**Maximum random background N_B (cts.)**	$N_{B,intr.}$ eq.(A11) $\eta = 4$ (cts.)	**Ambient flux outside main shielding [1] (n+γ)/(cm²s)** **Tolerable**	**Estimated [31]**
$5\cdot10^6$	$5\cdot10^3$	100	500	3	**7.3**	1	**30**	**$1\cdot10^{-5}$**
$1\cdot10^8$	$1\cdot10^5$	10	1000	12	**960**	50	**$2\cdot10^3$**	**$2\cdot10^{-4}$**
$5\cdot10^{10}$ [2]	$1\cdot10^6$	5	5000	50	**$2\cdot10^4$**	$2.4\cdot10^3$	**10^4**	**$1\cdot10^{-1}$**

[1] The ambient neutron and gamma fluxes refer to the energy range 0.5 to 10 MeV.

[2] An automatic control scheme for reduction of scatter foil volume will be used during high fluxes, see Sec. V.D.

A. C. Discussion and conclusion

The accuracy in the random background is derived from measurements of the counts in the two detectors and is therefore based on better statistics than had it been evaluated from the spectrum itself. Operation of the time-of-flight neutron spectrometer up to a spectrometer count-rate of 10^6 c/s is feasible in spite of the restriction imposed by the intrinsic background. The maximum tolerable random background counts over signal counts, varies from 0.01 to 4 over a temperature range from 3 to 50 keV. The total random background counts (within $\Delta\tau$=30 ns) must not exceed $2\,10^4$ for 5000 signal counts. This leaves room for the ambient background at the position of the D_1 detector of up to 10^4 $(n+\gamma)/(cm^2s)$. However, such levels would cause high count-rate saturation in the timing electronics. The practical limit is therefore approximately 10^3 $(n+\gamma)/(cm^2s)$, i.e. still orders of magnitude above the estimated flux outside the main shielding. Located in this position the spectrometer will also fulfil all ITER measurement requirements.

REFERENCES

[1] K. Tombaechi, J.R. Gilleland, Yu.A. Sokolov, R. Tosci and the ITER team, "ITER Conceptual Design", Nuclear Fusion, Vol. 31.No.6 (1991). ITER Joint Central Team, "Parameters of the ITER EDA Design", Plasma Phys. Control. Fusion 35 (1993) B23.

[2] O.N. Jarvis, "Neutron measurement techniques for tokamak plasmas", Plasma Phys. Control. Fusion 36 (1994),209-244.

[3] "Minutes of 1st Meeting", Physics Expert Group on Diagnostics. July 18-22, 1994; ITER Joint Work Site, San Diego, USA. SCX M1 94-08-03 F1.

[4] V. Mukhovatov, H. Hopman, S. Yamamoto, K. M. Young, P. Stott et.al., "ITER Diagnostics", ITER Documentation series, No. 33, International Atomic Energy Agency, Vienna, 1990.

[5] V. Parail, JET Joint Undertaking. Private communication, October 1994.

[6] J. Weiland, Dept. of Electromagnetic Field Theory, Chalmers University of Technology, Goteborg, Sweden. Private communication, October 1994.

[7] J. Scheffel, "Neutron spectra from beam-heated fusion plasmas", Nucl. Instr. and Meth. 224 (1984) 519-531.

[8] H. S. Bosch, "Review of Data and Formulas for Fusion Cross-sections", Report IPP I/252, Max-Planck Institut für Plasmaphysik, Garching bei Munchen 1990.

[9] H. Brysk, "Fusion Neutron Energies and Spectra", Plasma Physics, Vol. 15, (1973),611-617.

[10] O. N. Jarvis, "Neutron Detection Techniques for Plasma Diagnostics", Proceedings of the Course "Diagnostics for Fusion Reactor Conditions". EUR 8351-1 EN Vol. 1, Sept. (1982).

[11] N. S. Garis, R. Chakarova and T. Elevant," Simulation of particle transport in a novel 14 MeV neutron time-of-flight spectrometer". CTH-RF-97. Department of Reactor Physics. Chalmers University of Technology, S-412 96, Goteborg Sweden. ISSN 0281-9775.

[12] N. Hawkes, Harwell Laboratories, U.K. Private communication, June 1995.

[13] T. Elevant, N. Garis, R. Chakarova and P. Linde'n, "A neutron spectrometer for ITER". Rev. Sci. Instrum. 68 (1), January 1994.

[14] G. Grosshog, Dan Aronsson, K-H Beimer, L-O Pekkari,R. Rydz, O. Skeppstedt and N-G. Sjostrand, " The Use of the Neutron-Proton Scattering Reaction for D-T Fusion Spectrometry", Nucl. Instr. Meth., A249 (1986), 468.

[15] K. Drozdowicz, M. Hoek and D. Aronsson," Energy Calibration of Neutron Detectors for Neutron Spectrometer TANSY", Nucl. Instr. and Meth., A306 (1991), 315.

[16] M. Hoek, N. S. Garis, G. Grosshog," Simulation of the neutron and proton transport in the 14 MeV neutron time-of-flight spectrometer TANSY", Nucl. Instr. and Meth. A322, 248 (1992).

[17] J. Kallne and H. Enge,"Magnetic Proton recoil spectrometer for fusion plasma neutrons", Nucl. Instr. and Meth. A311 (1992) 595.

[18] T. Iguchi et.al., "Conceptual design of neutron diagnostic systems for fusion experimental reactor", Fusion Engineering and Design 28 (1995) 689.

[19] T. Elevant et al., "Silicon surface barrier detector for fusion neutron spectroscopy", Rev. Sci. Instrum. 57 (8) August (1986).

[20] F. Borchelt et. al., "First measurements with a diamond microstrip detector", Nucl. Instr. and Meth., A 354 (1995) 318-327 and A. V. Krasilnikov, "Diamond detector based DT neutron spectrometer for ITER", Proceedings of the International School of Plasma Physics "Piero Caldirola" workshop on Diagnostics for ITER, Aug. (1995), Plenum Press.

[21] T. Elevant et. al., "Scintillating Fibre Neutron Spectrometer", Proceedings of the International School of Plasma Physics "Piero Caldirola" workshop on Diagnostics for ITER, Aug. (1995), Plenum Press.

[22] M. Adinolfi et. al., "Progress on high-resolution tracking with scintillating fibres: a new detector based on capillaries filled with liquid scintillator", Nucl. Instr. and Meth. A315 (1992) 177.

[23] "Effects of Radiation on Materials and Components", John F. Kircher and Richard E. Bowman. Reinhold Publishing Corporation, New York. See also J.F. Baur et. al., "Radiation Hardening of Diagnostics for Fusion Reactors", General Atomic Company, GA-A16614 UC-20, (1981).

[24] Y. Yariv et. al., "Simulations of Neutron Response and Background Rejection for a Scintillating-fiber Detector", Nucl. Instr. and Meth., A292 (1990) 351.

[25] T. Elevant and M. Olsson et al., "The JET neutron time-of-flight spectrometer", Nucl. Instr. and Meth., A306, (1991) 331.

[26] T. Elevant, P. v. Belle, G. Grosshög, O.N. Jarvis, M. Olsson, G. Sadler, "The new JET 2.5-MeV neutron time-of-flight spectrometer", Review of Scientific Instruments, Vol. 63, No.10 (Part II), October (1992).

[27] T. Elevant, P van Belle, O. N. Jarvis and G. Sadler, "Measurements of Fusion Neutron Energy Spectra at JET by means of Time-of-Flight Techniques", JET-P(94) 53, November 1994. Nucl. Instr. and Meth., A364 (1995) 333-341.

[28] K-H. Beimer, "Studies of Neutron Measurement Methods for Fusion Plasma Diagnostics", Department of Reactor Physics, Chalmers University of Technology, Dissertation Thesis (1986).

[29] E. A. Straker, "Fast-Neutron Collimator Studies. TSF-SNAP core mapping collimator", Nucl. Appl., 6, (1969) 168, and D. W. Glasgow et. al., "Shielding for fast neutron scattering experiments of high sensitivity", Nucl. Instr. and Meth. 114 (1974) 521.

[30] Statististical textbook, e.g., "An Introduction to the Theory of Statistics", The Late G. Udny Yule and M. G. Kendall, Fourteenth edition, Third Impression, Charles Griffin & Company Limited, London, 1958.

[31] V. Sakharov, I. V. Kurchatov Institute of Atomic Energy, Moscow, USSR. Private communication, June (1989).

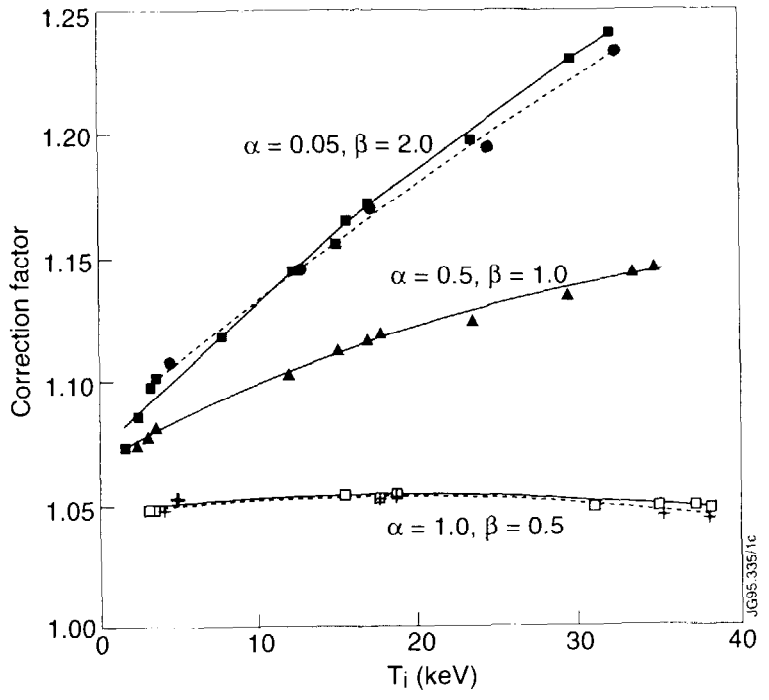

Fig.1: Correction factors $C(T_i^{obs})=T_i^{max}/T_i^{obs}$ for different parabolic plasma density (α) and temperature (β) profiles. T_i^{max} is the maximum temperature along a line-of-sight and T_i^{obs} denotes the ion temperature calculated from the accumulated neutron spectrum.

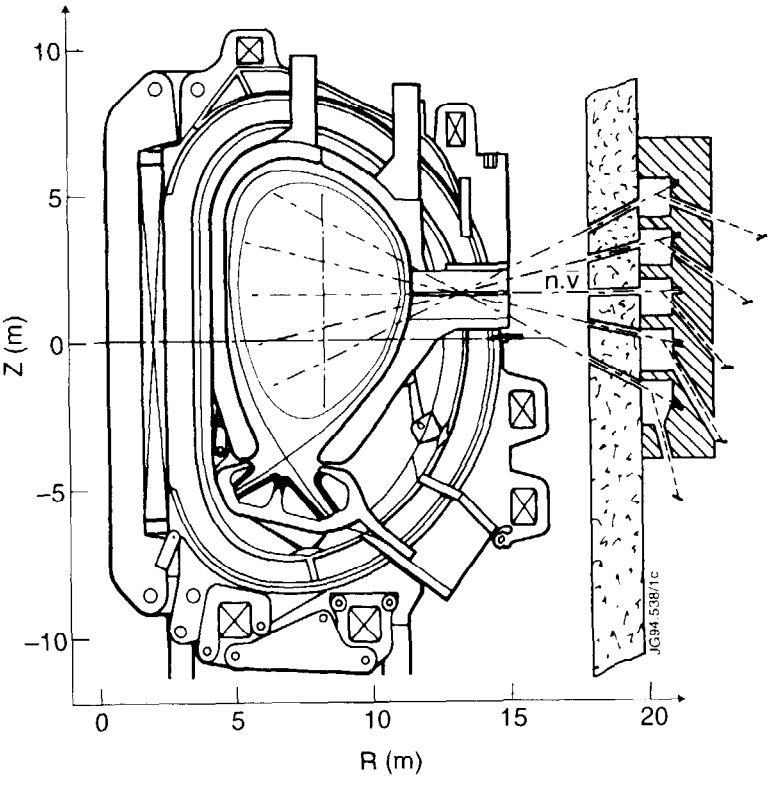

Fig.2: The ITER over all geometry is shown with an array of (5) Time-of-Flight neutron spectrometers for measurements of ion temperature profiles.

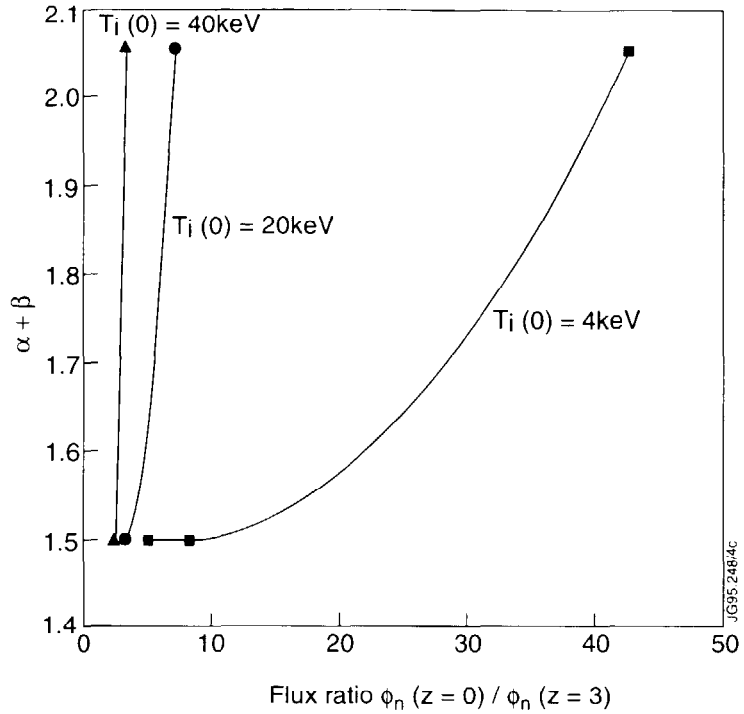

Fig.3: Diagram showing relation between profile 'peakedness' $\alpha+\beta$ versus the flux ratio $\Phi_n(z=0)/\Phi_n(z=3)$. From left to right the curves correspond to on-axis ion temperatures of 40, 20 and 4keV, respectively. The standard ITER equilibrium of fig.1 is used.

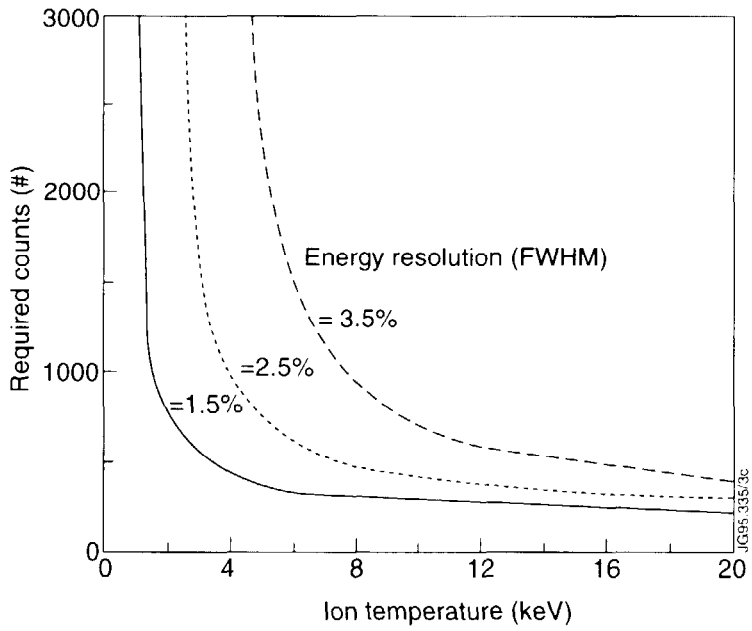

Fig.4: The minimum required number of counts[11] as a function of ion temperature for energy resolution equal to 1.5%, 2.5% and 3.5% and for $\Delta T_i/T_i=10\%$.

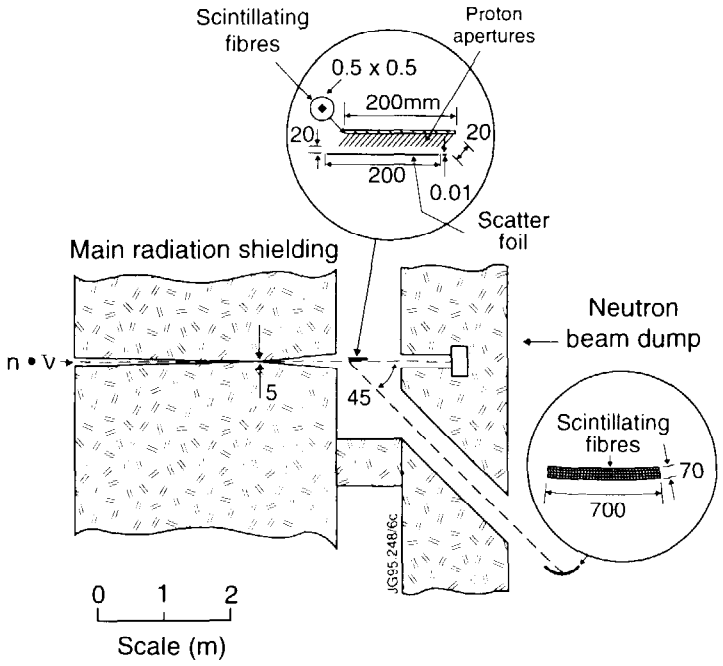

Fig.5: Details of the Time-of-Flight spectrometer are shown with collimator, scatter foil, apertures, beam dump and detectors.

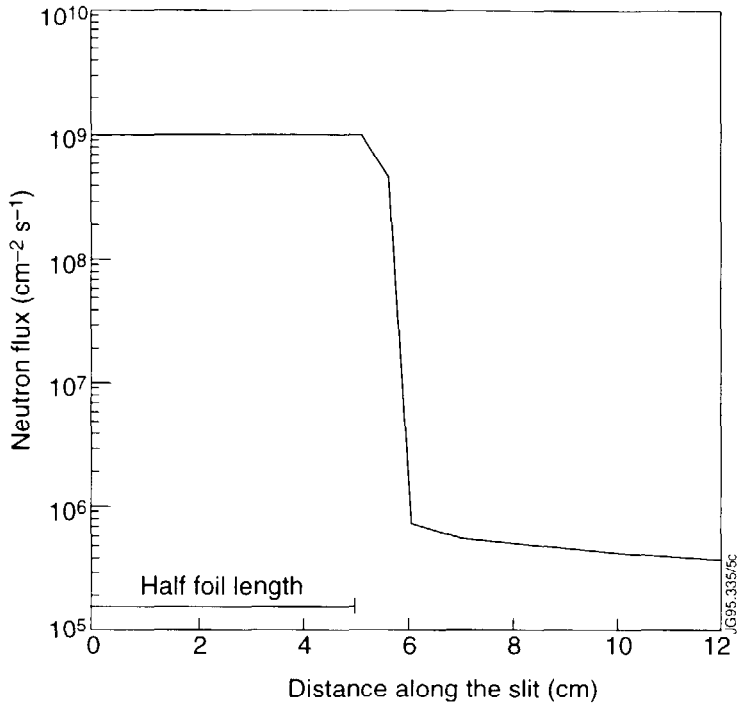

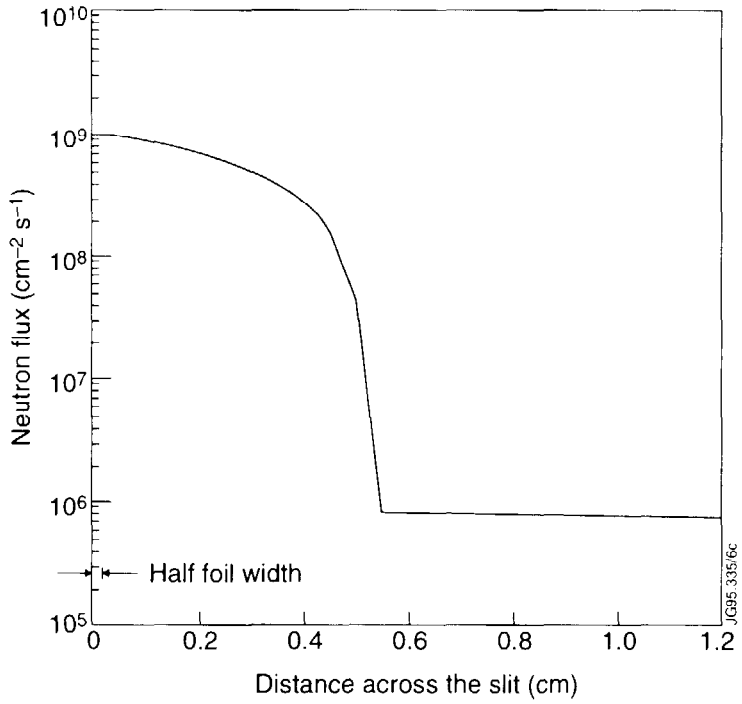

Fig.6: Neutron flux is shown a) across the collimator slit and b) along the slit. The waist dimensions are 1.0•10cm^2.

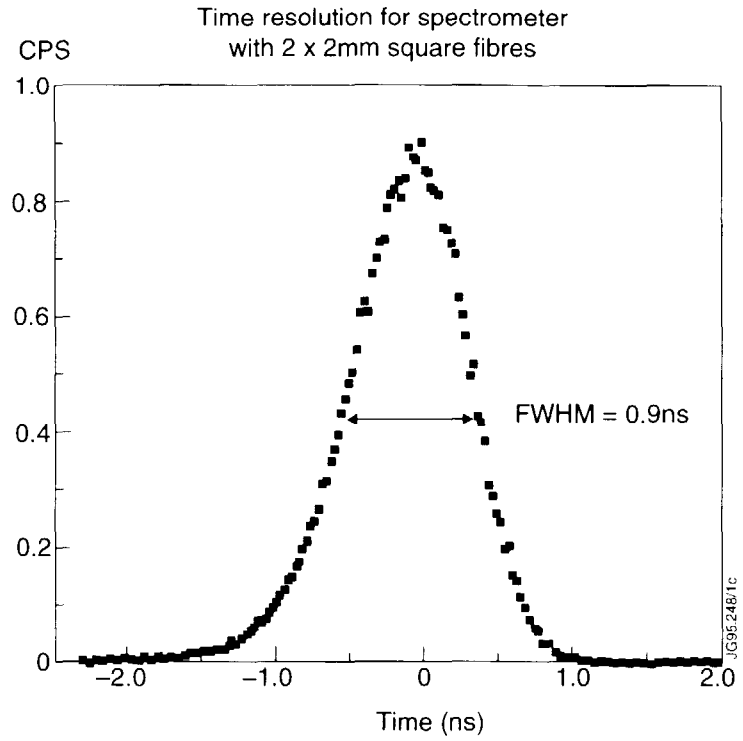

Fig.7: Time resolution measured with 0.2•0.2•70cm³ square scintillating fibres.

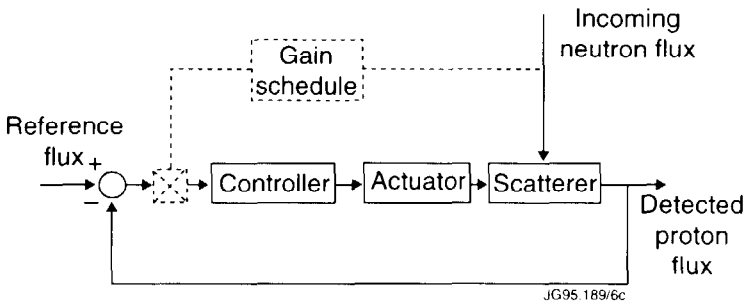

Fig.8: Flow chart of proposed control system for scattered neutron flux.

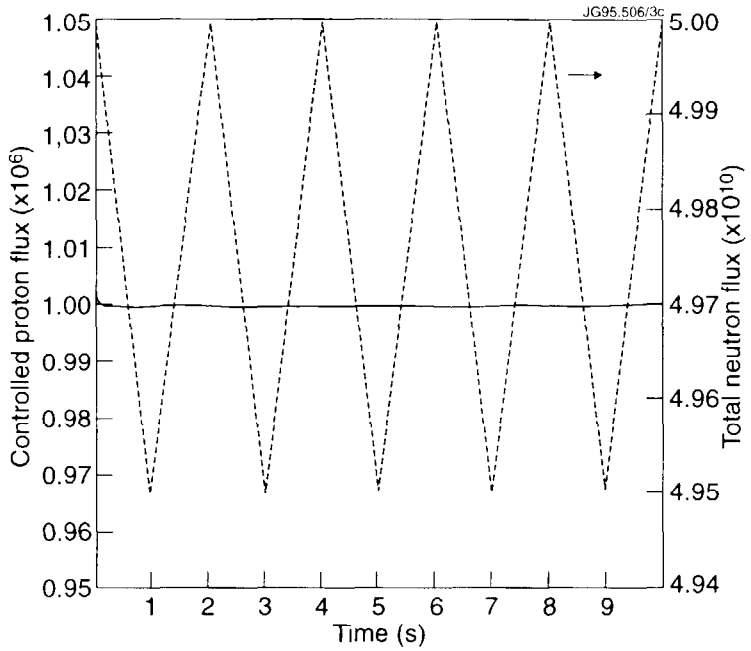

Fig.9: Neutron and controlled D_0 count-rate at high neutron flux level..

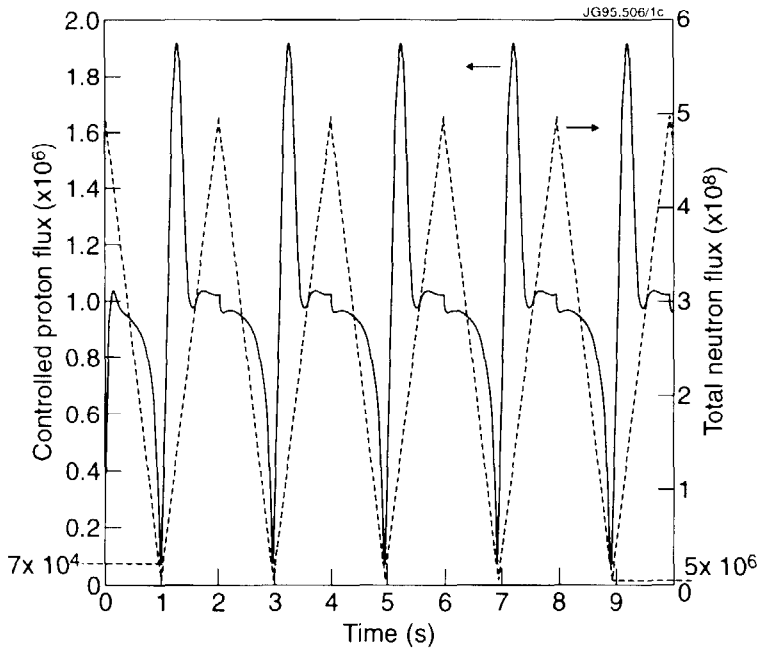

Fig.10: Neutron flux and controlled D_0 count-rate with unscheduled controller.

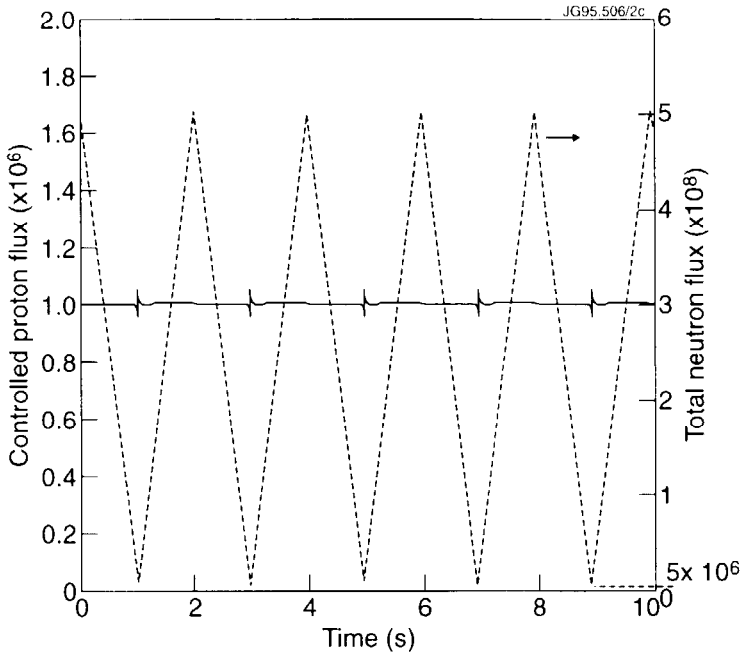

Fig.11: Neutron flux and controlled D_0 count-rate with scheduled controller.